Supplementary Materials

Atmospheric API-CIMS:

The atmospheric API-CIMS is a downsized version of the instrument used and described by Marandino et al. (2007). A schematic of the main components is given in Figure S1. The ion source consists of a heated and temperature-controlled glass-lined stainless steel tube containing a radioactive ^{63}Ni foil, as described in Saltzman et al. (2009). Lens voltages for ion optics were supplied by a Gamma custom multichannel DC power supply and the quadrupole supply was an Extrel QPS500 DC/RF power supply and mass command board. Ions were detected using an ion multiplier and discriminator/preamplifier. The primary difference between this instrument and the earlier CIMS instrument is the replacement of a turbo-pumped vacuum stage (1000 L s^{-1}; 5 x 10^{-3} Torr) in the vacuum system with a turbo charger/rough pumped (50 L s^{-1}; 1 Torr) collision chamber. The collision chamber is an Extrel API collision chamber with modified entrance configuration. A custom Labview™ program and multichannel A/D interface (NI USB-6343, X Series DAQ) were used to provide the mass command signal and to acquire the ion counts. The same interface was used to acquire the saw tooth synchronizing signal and to output the ion counts as analog signals for logging by the multichannel data logger described above.

The gas standard was supplied from a cylinder (11.79 ppm) at a mass flow-controlled flow rate of 3-6 ml min^{-1}, resulting in a d3-DMS level of 440 – 885 ppt in the air stream. The gas standard was delivered using 1/32″ ID Teflon tubing and a low volume 3-way solenoid valve located at the base of the foremast. Gas flow rates were controlled and logged via a custom PC-controlled 8-channel mass flow controller circuit board.

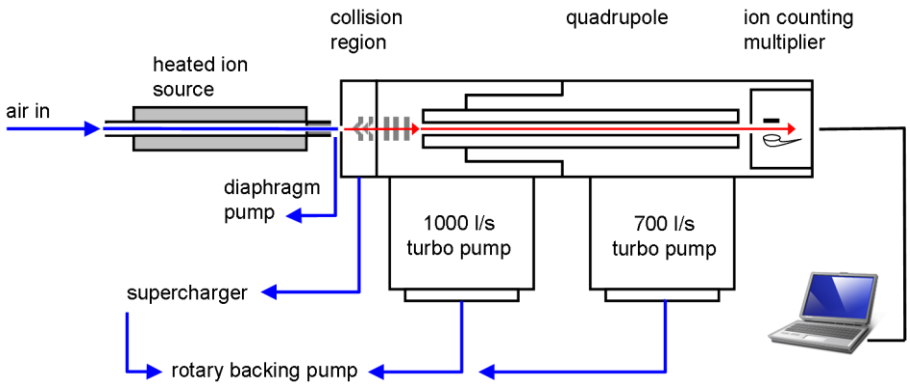

Figure S1: mesoCIMS instrument schematic

DMS gas standards:

Isotopically-labeled DMS gas standards in the range of 1-10 ppm were prepared by injecting liquid d3-DMS (Cambridge Isotope Laboratory) into dry, evacuated 6 L high pressure aluminum cylinders. The cylinders were pressurized to 1000 psi with N_2. Three cylinders were used to calibrate the API-CIMS instruments on the Knorr_11 cruise. These were calibrated against a temperature-controlled, gravimetrically calibrated permeation tube (Vici Metronics) in the laboratory before and after the cruise and intercompared during the cruise.

The gas standard used for atmospheric DMS measurements and the aqueous DMS standard used for seawater measurements were regularly intercompared during the cruise. This was done by stopping the flow of aqueous d3-DMS standard and introducing a gas standard into the air stream from the seawater equilibrator for a period of 5 minutes every 2 hours. Seawater DMS concentrations were calculated using the gas standard assuming that air and seawater were fully equilibrated in the equilibrator. We compared the seawater DMS concentrations from the gas standards (DMS_{gas}) to the adjacent measurements using the liquid standard (DMS_{liq}). The mean ratio of these measurements (DMS_{gas} / DMS_{liq}) was 1.07±0.18 (1σ, n=52). The variance in the ratio includes a contribution from temporal variability in ambient DMS, as the two measurements were offset by several minutes.

DMS Flux Quality Control:

DMS flux intervals that met any of the following criteria were excluded:

- $F_{sum} \geq 0.45$ at $f_{norm} = 0.027$ (0.02 Hz at U_{10n}=10 m s^{-1})
- $F_{sum} \leq 0$ at $f_{norm} = 0.014$ (0.01 Hz at U_{10n}=10 m s^{-1})
- $F_{sum} \geq 1.05$ at $f_{norm} = 0.73$ (1 Hz at U_{10n}=10 m s^{-1}).

Flow distortion:

Field measurements and computational fluid dynamics simulations demonstrate flow distortion and vertical displacement of flow fields over the bow of research vessels (Yelland et al., 2002). The magnitude of this effect varies as a function of relative wind direction and can have a significant impact on the measurement of momentum flux or drag coefficients. To minimize this effect, a variety of wind sector limits have been used in previous shipboard

eddy covariance gas exchange studies: ±120° (Blomquist et al., 2006); ±50° (Huebert et al., 2010); and ±60° (Marandino et al., 2007; Yang et al., 2011).

On Knorr_11, flow distortion was indicated by the presence of an apparent positive mean vertical wind measured by the sonic anemometers after correction for ship motion and sensor orientation but prior to coordinate rotation (Figure S2a). Flow distortion was also indicated by systematic variations in horizontal wind speed measured at various heights on the foremast, reflecting vertical displacement of the winds. Horizontal wind speed differences of up to 4 m sec^{-1} were found between our sensors and the ship's 2D sonic and cup anemometers mounted 2 meters higher on the foremast (Figure S2b). The highest sensor should experience the least flow distortion, so the ship's 2D sonic winds were used to calculate U_{10}. Transfer coefficients for momentum (C_{D10}) and sensible heat (C_{H10}) were computed using fluxes from our sonic anemometers and U_{10} from the ship's 2D sonic winds. Transfer coefficients computed in this way show good agreement with those calculated using the COARE model (Figure 5a).

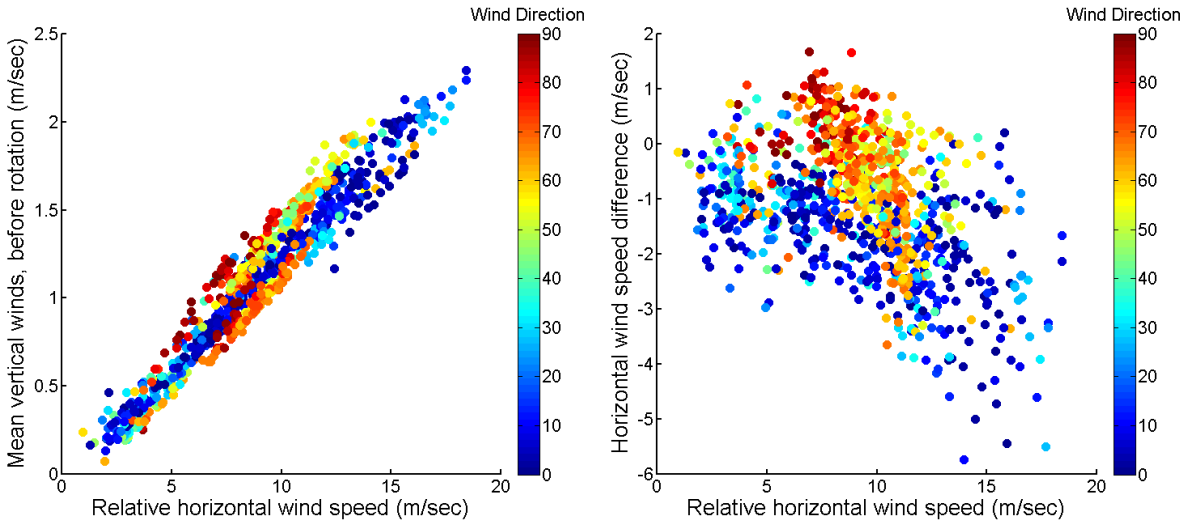

Figure S2: Evidence of flow distortion on the Knorr_11 foremast. Left panel: Mean vertical wind speed before coordinate rotation vs. relative horizontal wind speed, with symbol color indicating apparent absolute wind direction relative to the bow. Right panel: difference in horizontal wind speed. CSAT3 sonic (13.6 m height) minus ship's 2D sonic (15.5 m height), with symbol color indicating apparent absolute wind direction relative to the bow.

The influence of relative wind direction on momentum flux and gas flux was examined during a portion of the cruise where the relative wind direction varied while wind speed

(U_{10n}) and DMS_{sw} remained fairly constant (DOY 184.5-187, U_{10n} = 9.7±1.4 m s^{-1}; DMS_{sw} = 4.0±1.9 nM). Frequency distributions of Dalton number ($\mathcal{D}_{660} = k_{660}/U_{10n}$) and the drag coefficient ($C_{D10} = w'u'/U_{10n}^2$) for relative wind sectors ±0-30°, ±30-60°, and ±60-90° are shown for this period in Figure S3. The data show no statistically significant bias between the relative wind sectors for $\mathcal{D}_{660}$ or C_{D10} (unequal variance t-test; $\alpha < 0.01$). These results suggest that flow distortion on the R/V Knorr bow mast is a relatively small source of variance in D_{660} and C_{D10} at least during this period of fairly constant conditions. In this paper, data from ±0-90° are presented.

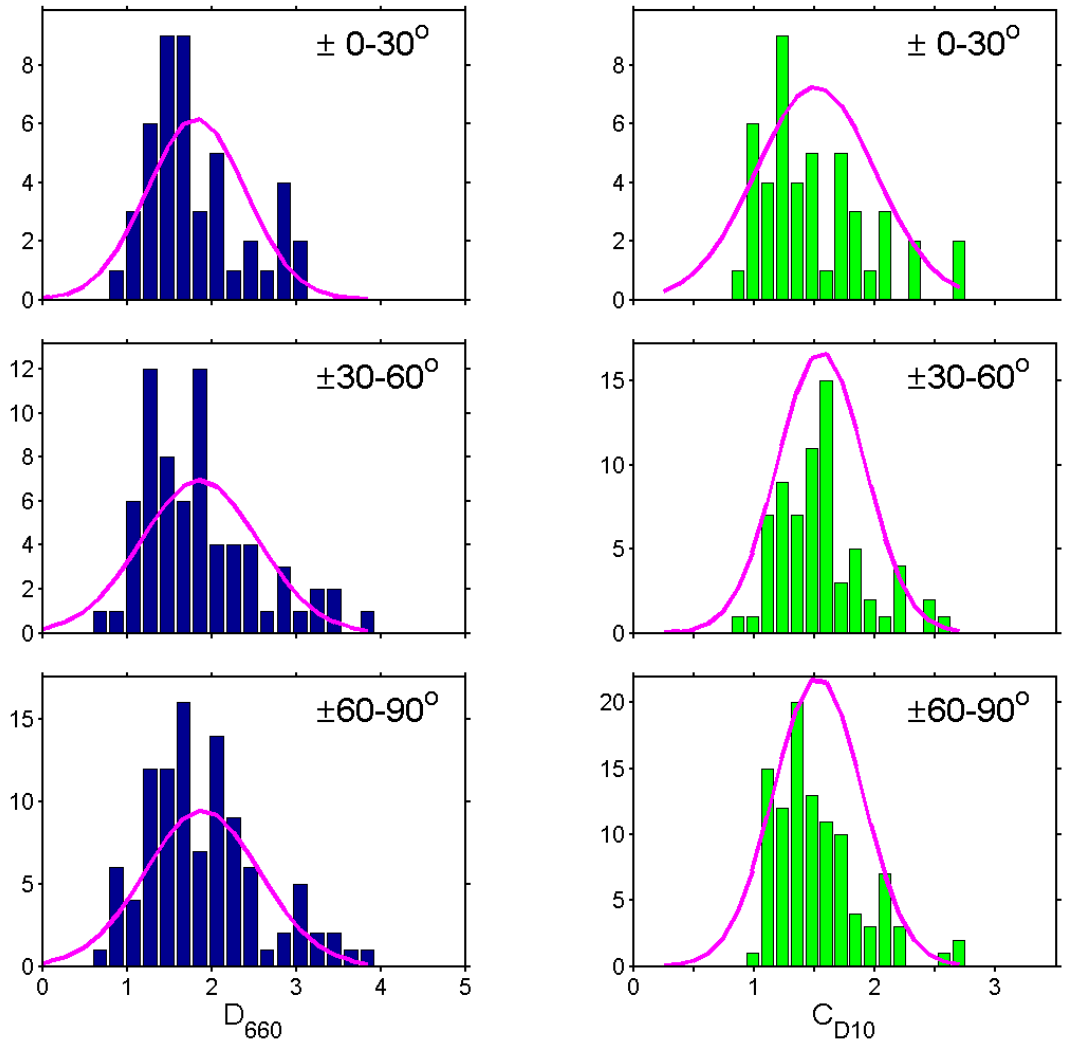

Figure S3: Frequency distribution of $\mathcal{D}_{660}$ (left, cm s hr^{-1} m^{-1}) and C_{D10} (right) from Knorr_11 DOY 184.5-187. Data is shown for three relative wind direction sectors: ±0-30°, ±30-60°, and ±60-90°.

Soloviev (2007) model calculation:

In this equation, k_{int} has units of m/s:

$$k_{\mathrm{int}} = u_* A_0 \Lambda_0^{-1} Sc^{-0.5} \left(1 - a_0^3 \Lambda_0^4 Rf_0\right)^{0.25} \left(1 + Ke/Ke_{CR}\right)^{-0.5} \left(660/Sc\right)^{-0.5}$$

u_* Waterside friction velocity (derived from COAREv3.1 airside friction velocity, converted to waterside units using water and air densities)

A_0 0.92 (see Soloviev, 2007)

Λ_0 7.4 (see Soloviev, 2007)

S_C Schmidt number for DMS (calculated according to Saltzman et al., 1993)

a_0 0.25 (see Soloviev, 2007)

$$Rf_0 = \frac{\alpha_T g_i \nu}{c_P \rho u_*^4} \left(Q_E + Q_T - I_L + \frac{\beta_S S_0 c_P}{\alpha_T L} Q_E \right)$$

α_T Thermal expansion coefficient (2.2×10^{-4} °C^{-1})

g_i Acceleration due to gravity (9.80665 m/s^2)

ν Kinematic viscosity of seawater (1.05×10^{-6} m^2/s)

C_P Specific heat capacity of water (4×10^3 J/kg C)

ρ Density of seawater (kg/m^3)

Q_E Latent heat flux (W/m^2) from COAREv3.1 model, with sign reversed so positive sea-to-air flux.

Q_T Sensible heat flux (W/m^2) from COAREv3.1 model, with sign reversed so positive sea-to-air flux.

I_L Downward longwave irradiance (W/m^2) from COAREv3.1 model, with sign reversed so positive sea-to-air flux.

β_S Haline expansion coefficient (8×10^{-4} psu^{-1})

S_0 Seawater salinity (unitless)

L Latent heat of vaporization (2.6×10^6 J/kg)

$$Ke = u_*^3 / g_i \nu$$

$$Ke_{CR} = Rb_{CR} \frac{\nu_a}{\nu} \left(\frac{\rho_a}{\rho} \right)^{3/2} \frac{1}{A_W}$$

Rb_{CR} Critical breaking wave parameter describing wind-wave breaking (10^3), which corresponds to Ke_{CR}=0.18 at wave age Aw=3.25 (Zhao and Toba, 2001; Soloviev, 2007)

ν_a Viscosity of air = $1.326\times10^{-5}(1 + 6.542\times10^{-3}\, t + 8.301\times10^{-6}\, t^2 - 4.84\times10^{-9}\, t^3)$

where t = air temperature (°C)

ρ_a Density of air (kg/m^3)

$$A_W = g_i / \left(\omega_P u_{*a}\right)$$

u_{*a} Airside friction velocity (derived from COAREv3.1)

ω_P Peak angular frequency of waves, $2\pi F_P$, where F_P is the peak wave frequency (s^{-1})

References

Blomquist, B. W., Fairall, C. W., Huebert, B. J., Kieber, D. J., and Westby, G. R.: DMS sea-air transfer velocity: Direct measurements by eddy covariance and parameterization based on the NOAA/COARE gas transfer model, Geophys. Res. Lett., 33, art. no.-L07601, 10.1029/2006gl025735, 2006.

Huebert, B. J., Blomquist, B. W., Yang, M. X., Archer, S. D., Nightingale, P. D., Yelland, M. J., Stephens, J., Pascal, R. W., and Moat, B. I.: Linearity of DMS transfer coefficient with both friction velocity and wind speed in the moderate wind speed range, Geophys. Res. Lett., 37, 10.1029/2009gl041203, 2010.

Marandino, C. A., De Bruyn, W. J., Miller, S. D., and Saltzman, E. S.: Eddy correlation measurements of the air/sea flux of dimethylsulfide over the North Pacific Ocean, Journal of Geophysical Research-Atmospheres, 112, D03301, 2007.

Saltzman, E. S., King, D. B., Holmen, K., and Leck, C.: Experimental determination of the diffusion coefficient of dimethylsulfide in water, J. Geophys. Res.-Oceans, 98, 16481-16486, 1993.

Saltzman, E. S., De Bruyn, W. J., Lawler, M. J., Marandino, C. A., and McCormick, C. A.: A chemical ionization mass spectrometer for continuous underway shipboard analysis of dimethylsulfide in near-surface seawater, Ocean Science, 5, 537-546, 2009.

Soloviev, A. V.: Coupled renewal model of ocean viscous sublayer, thermal skin effect and interfacial gas transfer velocity, Journal of Marine Systems, 66, 19-27, 10.1016/j.jmarsys.2006.03.024, 2007.

Yang, M., Blomquist, B. W., Fairall, C. W., Archer, S. D., and Huebert, B. J.: Air-sea exchange of dimethylsulfide in the Southern Ocean: Measurements from SO GasEx compared to temperate and tropical regions, J. Geophys. Res.-Oceans, 116, 10.1029/2010jc006526, 2011.

Yelland, M. J., Moat, B. I., Pascal, R. W., and Berry, D. I.: CFD model estimates of the airflow distortion over research ships and the impact on momentum flux measurements, Journal of Atmospheric and Oceanic Technology, 19, 1477-1499, Doi 10.1175/1520-0426(2002)019<1477:Cmeota>2.0.Co;2, 2002.

Zhao, D., and Toba, Y.: Dependence of whitecap coverage on wind and wind-wave properties, J Ocean, 57, 603-616, 2001.